International Journal of Mechanical Sciences 134 (2017) 234–243

Contents lists available at ScienceDirect

International Journal of Mechanical Sciences

journal homepage: www.elsevier.com/locate/ijmecsci

Effect of nodal mass on macroscopic mechanical properties of nanoporous metals

J. Jiao[a,*], N. Huber[a,b]

[a] Institute of Materials Research, Materials Mechanics, Helmholtz-Zentrum Geesthacht, Germany
[b] Institute of Materials Physics and Technology, Hamburg University of Technology, Germany

ARTICLE INFO

Keywords:
Nanoporous metal
Finite element method
Nodal mass
Macroscopic response
Scaling laws
Size dependent strength

ABSTRACT

The current work investigates the effect of the nodal mass on the macroscopic mechanical behavior of nanoporous metals using the Finite Element Method. A nodal corrected beam modeling concept is introduced that allows local incorporation of the effective elastoplastic mechanical behavior of the nodal mass in the nodal area of a representative volume element (RVE). The calibration to the corresponding Finite Element solid model is achieved by integrating additional geometry and material parameters to the so-called nodal areas in the beam model. With this technique an excellent prediction can be achieved over a large range of deformation for different types of RVEs. From the results of the nodal corrected beam model, modified leading constants are determined in the scaling laws for Young's modulus and yield strength. The effect of the nodal correction is also studied with respect to various randomization levels. Finally, the ligament size dependent strength is analyzed by applying the proposed model to experimental data. It could be shown that the nodal correction improves the overall agreement with literature data, particularly for such data points that are related to samples with a high solid fraction.

1. Introduction

Nanoporous gold (NPG) made by de-alloying can be produced as macroscopic objects that exhibit a bi-continuous network of nanoscale pores and solid 'ligaments' which are connected in nodes. The solid fraction φ of the porous body is approx. 30% [1–4]. φ is used as the major parameter in several theoretical models for predicting the macroscopic mechanical behavior of the porous materials [5–9]. The Gibson-Ashby model [10], as the most commonly used one among these models is reported to significantly overestimate the macroscopic mechanical response of nanoporous metals [11–14]. The overestimation indicates that the mass utilization for deformation in such a material is not as efficient as assumed by the Gibson-Ashby structural model for open pore foams.

In a wider spectrum of attempts for understanding the extraordinary mechanical responses of nanoporous metals, extensive modeling approaches have been conducted. Atomistic and molecular dynamics simulations have been implemented to investigate the deformation behavior under tension and compression [6,15–17]. It was found that the surface stress has a substantial impact on the tension/compression asymmetry, anomalous compliance and early yield. The simulations reported in [16] revealed significant stacking fault formation and dislocation accumulation within the nanosized ligaments, confirming the existence of substantial work hardening under plastic deformation as suggested in [8]. Further modeling work on the microstructural and continuum level [18,19] was conducted to explore the origin of the unusual low Poisson's ratio observed during macroscopic compression of nanoporous gold samples. It was found that on the one hand the elastic Possion's ratio is independent of the ligament size but decreases with increasing degree of randomization through an increasing percentage of torsion of the ligaments [18]. On the other hand, the plastic Poisson's ratio showed a strong dependency on the ligament size, which could be successfully reproduced with the Deshpande–Fleck model [19].

Other works [20–23] that studied surface elasticity or surface boundary conditions have been conducted aiming to explain the macroscopic mechanical behaviors of this material from a microscopic point of view, with a particular emphasis on size effects. Very recently, the signature of the surface energy was studied by combining macroscopic compression experiments with a Finite Element beam model of a randomized diamond structure, enriched by coaxial thin-walled tubular elements for modeling a switchable surface stress [24]. The results showed in conjunction with the experimental findings that, contrary to the elastic Poisson's ratio, the plastic Poisson's ratio responds strongly to electrical surface modulation. This behavior was identified as the signature of a surface-induced tension-compression asymmetry of the flow stress

* Corresponding author.
E-mail address: jingsi.jiao@hzg.de (J. Jiao).

https://doi.org/10.1016/j.ijmecsci.2017.10.011
Received 23 June 2017; Received in revised form 20 September 2017; Accepted 7 October 2017
Available online 9 October 2017

at the level of individual ligaments. In summary, the discussed highly efficient Finite Element beam models provide valuable insights into the mechanisms that control macroscopic strength and modulus, as well as elastic and plastic Poisson's ratio in dependence of solid fraction, randomization and surface energy. Further work should be aimed towards modeling structures that are more realistic. To begin with, the local incorporation of the nodal mass into the structure appears to be among the most relevant points.

Attempts for interpreting the significant discrepancy between the prediction of Gibson-Ashby model and experimental results have also been the scope of the recent researches. In the works of [8,9,12,25], the network structure was significantly simplified to unit cell structures, such as cubic, diamond or three-point bending beam. In extension to the Gibson-Ashby model, an additional parameter that incorporates the size of the nodes connecting the ligaments is introduced in these refined models. The extra mass of the nodes is investigated regarding the calculation of the solid fraction φ and the mechanical response of the unit cell. It is concluded that the nodal mass should be counted as another important factor that is associated with the relation between aspect ratio of the ligaments, solid fraction and macroscopic mechanical properties. More specifically, it was indicated that the discrepancy between the experimental measurements and the Gibson-Ashby model prediction is due to that there is a massive mass accumulated at the nodes, which does not contribute to the elastic deformation of the unit cell [9,12,25].

The effect from the nodes on the elastic-plastic deformation was investigated by comparing results from finite element simulations for a finite element solid model with spherical nodes and a finite element beam model, that reduces the nodes to a coupling constraint of the connected beam elements, based on the diamond unit cell [8]. It was found that the elastic stiffening caused by the nodes is partially compensated by the effect of increasing shear deformation for thick ligaments. Concerning the plastic deformation behavior, the shortening of the ligament length due to the nodal mass was identified as an important effect that was incorporated as a correction factor in the proposed scaling laws. Thus, for the scaling law of the macroscopic mechanical behavior, the structural arrangement of the ligaments is not the only influential parameter; the different approaches for modeling the nodes in terms of their contribution to the solid fraction as well as elastic and plastic deformation behavior will also lead to different scaling laws compared to the Gibson–Ashby model.

The studies on nanoporous metals cannot be restricted to a simplified, geometrically perfect unit cell structure, due to that the real structure of nanoporous metals is a spatial network structure with complex topological and morphological characteristics [7,13,26,27]. In order to investigate the structural parameters and obtain a more realistic deformation of the ligaments, highly generalized beam elements are used, which offer excellent computational efficiency even with thousands of ligaments modeled in a representative volume element (RVE). Based on the diamond lattice structure that was established in the work of [8] and further refined by [29], the effects of ligament shape variation and randomization on the various deformation modes of bending, torsion, and tension/compression was investigated [18]. It could be shown, that the beam element B31 in ABAQUS [28] is capable of capturing all fundamental deformations for even thick beams with a ligament radius to length ratio, r/l, up to 0.5 corresponding to a solid fraction of 69%. So far one remaining drawback of the RVE built from beam elements is the unsolved question of how to model the mass in the nodal areas, because the ligaments in the model are conjugated at virtual nodes. This leads to a larger compliance and lower strength of the beam model. In the study of [29], a correction of the macroscopic yield strength was considered by increasing the yield strength of the solid phase by a factor that was derived from the available lever for bending of the ligament which is shortened by the nodal mass, based on the correction derived in [8]. It is however unclear, how accurate and how general this approach is, particularly when the RVE has increasing complexity through adding randomization or variations of ligament shape.

In the current work, a modeling concept is proposed to address the issue of modeling the connecting nodes without losing the advantages of the beam model. More specifically, the elastic-plastic response of a tetrahedron building block modeled with beam elements is adjusted with respect to the mechanical responses of a corresponding solid model under bending deformation. For the calibration, the beam elements in the nodal area are assigned with parameters defining geometry and mechanical properties that can differ from those of the ligaments.

The integration of these so-called nodal beam elements into the RVE of [29] aims at predicting both elastic and plastic mechanical behavior comparable to the RVE that is built with solid elements and correctly includes the nodal deformation behavior. Furthermore, the scaling relations between the solid fraction φ and the elastic-plastic properties of nanoporous metals based on the nodal corrected beam model are analyzed and compared to previous studies. Gibson-Ashby scaling laws for elasticity and plasticity with modified leading constants are proposed that incorporate the effect of the nodal mass on the macroscopic mechanical response. The role of the nodal mass on the macroscopic mechanical response is also analyzed with respect to various randomization levels. Finally, the ligament size dependent strength of nanoporous gold is determined by applying the proposed model to experimental data. The results are discussed in the light of previous studies [29].

2. Extension of the beam model

The goal of this section is to develop a RVE built with beam elements, where the mechanics of the connecting nodes is physically and locally included in each of the nodes of the beam structure. It shall serve for predicting the elastic-plastic macroscopic response of a nanoporous metal with high computational efficiency. This approach would allow eliminating the phenomenological correction factor that has limited accuracy and does not allow considering effects of local structural variations in the vicinity of the nodes.

In what follows, a beam nodal correction approach will be proposed that is based on a tetrahedron structure – the building block of the diamond structure – that allows studying the mechanical response on a more advanced level compared to a single ligament RVE. The tetrahedron structure serves for adjusting the elastic-plastic deformation behavior of the beam model in relation to a solid model of same geometry against bending. The approach will be validated with respect to torsion on the level of the tetrahedron structure and, in a second step, for larger RVEs that are compared to solid RVEs.

2.1. Tetrahedral building block

A tetrahedron structure consisting of four ligaments is sketched in Fig. 1. It serves as the fundamental building block for the RVE, proposed by [8]. Fig. 1a shows the structure modeled with solid elements. The geometry consists of the nodal area in form of a spherical mass connected with four ligaments, of which only half of the ligament is modeled. Fig. 1b demonstrates the equivalent structure that is modeled with beam elements. The ligaments are connected by their common node via linking all displacement and rotational degrees of freedom. As the nature of the beam model, the nodal area contains intersecting volumes of the ligaments. Thus, the solid fraction has to be calculated independent of the volume of the elements in the finite element model based on the initial geometry shown in **Fig. 1**a. While the calculation of the solid fraction can be easily carried out for the perfectly ordered diamond structure [8] and also for the randomized diamond structure [29], the correct mechanical response requires a modification of the beam model.

As bending is the dominant deformation mechanism in nanoporous metals, the calibration of the model parameters will be carried out for such a deformation. This is achieved by applying a transverse displacement w at the end of the top ligament while fixing the other three ligament ends in space (shown in **Fig. 1**a and b). The following approach

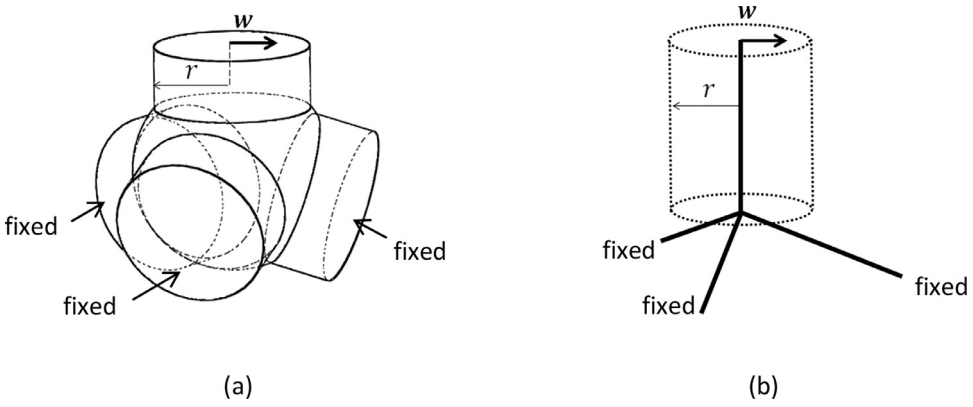

Fig. 1. Geometry of the tetrahedron building block for (a) solid model and (b) beam model.

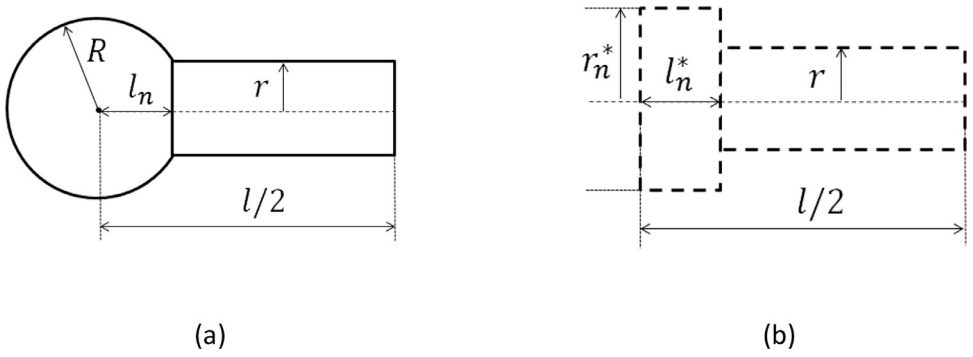

Fig. 2. Parameters defining the geometry of the ligament-nodal structure (a) solid model and (b) beam model.

Table 1
Geometry parameters and resulting solid fractions for simulations with variation of r/l and c_R.

$r/l=0.19$			$r/l=0.25$			$r/l=0.31$		
$c_R=1$	$c_R=1.05$	$c_R=1.1$	$c_R=1$	$c_R=1.05$	$c_R=1.1$	$c_R=1$	$c_R=1.05$	$c_R=1.1$
$\varphi=0.126$	$\varphi=0.127$	$\varphi=0.129$	$\varphi=0.207$	$\varphi=0.210$	$\varphi=0.214$	$\varphi=0.301$	$\varphi=0.307$	$\varphi=0.313$

aims at adjusting geometrical and material parameters of the beam elements in the nodal area, such that the mechanical response of the beam model is equivalent to that of the solid model.

For introducing the geometrical parameters of the modified beam model, one ligament with its connecting node is schematically shown in Fig. 2a and b. For the solid model in Fig. 2a, the parameters R and l_n are the nodal radius and the length between nodal center and the end of the ligament attached to the node, respectively. In the nodal corrected beam model, shown in Fig. 2b, r_n^* and l_n^* are adjustable geometrical parameters describing the larger cross-section of the beam elements in the nodal area and the length between the node center and the end of the ligament, respectively. The ligament radius r and ligament length l that is defined as the distance between the two node centers, are common parameters for the solid model and the beam model. Another parameter c_R is introduced, which is a constant governing the adjustable nodal mass by linking the ligament radius r and nodal radius R in the form of $R=\sqrt{3/2}\,c_R\cdot r$ [8].

All the calculations in the study are conducted with the FEA code ABAQUS/Implicit [28]. The geometry of the solid and the beam model is meshed with R3D3 and B31 elements. In Table 1 three r/l ratios and c_R values are listed that result in nine model realizations. The range of r/l is selected based on the range from the morphological study for the ligaments of NPG in the work of [9], which includes the typical range of the solid fraction of NPG from 0.25 to 0.3 [8,29]. A value of $c_R=1$ leads to the minimum possible size of the connecting node where the four ligaments touch, while $c_R=1.1$ is reported to represent a more realistic estimation of the node size in nanoporous metals [8].

To apply the same loading condition to the solid model as to the beam model, the solid ligament cross sectional surface (Fig. 1a) is coupled to a rigid plate with a 'Coupling' constraint that has a 'Continuum distribution'. The loading can be therefore assigned to the center point of the rigid plate and distributed to the whole surface [28], ensuring the maximum level of the similarity between the solid and beam models with respect to the load application [18].

The material behavior of the solid fraction is assumed to be elastic-perfectly plastic with a Young's modulus E_S of 81 GPa and a Poisson's ratio ν of 0.42. The yield strength $\sigma_{y,S}$ is 500 MPa and plastic deformation evolves without work hardening [8,29].

2.2. Calibration of the nodal beam elements

As mentioned in the previous section, the calibration of the beam model is conducted with the reference to the mechanical response of the solid model under bending deformation. Fig. 3 illustrates the von Mises stress distribution for a solid tetrahedron structure ($r/l=0.25$, $c_R=1.1$) under the transverse loading displacement w according to Fig. 1a that leads to plastic bending and shearing of the top ligament, but also of the upper part of the connecting node and its surrounding ligaments.

The correction for the mechanical response of the beam tetrahedron structure is carried out by firstly adjusting its additional geometrical parameters r_n^* and l_n^*. To that end, the stiffness of the tetrahedron (for both of the beam and solid models), $k=F/w$, is computed from the first loading increment in the elastic regime, such that the structure is undergoing only small elastic deformation. The strength F is read as the reaction force of the tetrahedron structure in the plastic regime when

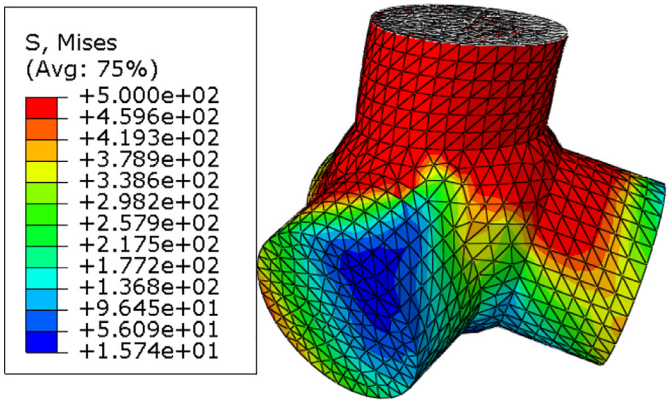

Fig. 3. Mises stress distribution of solid model with $r/l = 0.25$, $c_R = 1.1$; top ligament and upper part of the nodal mass and lower ligaments are plastically deformed.

$w/l = 0.017$. This deformation value leads to a macroscopic deformation within the plastic regime of the force displacement curve, which is sufficiently far from the elastic-plastic transition. The data k_{solid} and F_{solid}, determined from the solid model, are used as references for the calibration of the beam model's elastic and plastic response, represented by k_{beam} and F_{beam}, respectively. Fig. 4a shows the ratios of k_{beam}/k_{solid} (black crosses) and F_{beam}/F_{solid} (red circles) for the case of $r/l = 0.19$ and $c_R = 1.1$. The analyzis is conducted with systematically varying the parameters r_n^* and l_n^*; and it is done for all geometries listed in Table 1. The best fit is found where stiffness and strength results are simultaneously closest to the value of 1, represented by the yellow plane in Fig. 4a.

It can be seen from Fig. 4a that the stiffness k_{beam} smoothly increases with r_n^*. In contrast to that, the strength ratio first increases in the same way with r_n^* but then arrives at a plateau. This is because plastic yielding would always initiate at the end of the ligament once the nodal region is sufficiently strong. Until then, the nodal region also contributes to the plastic deformation, as shown in Fig. 3. The magnitude of the plateau is related to the lever length of the ligament that can be obtained in the form of $l - l_n^*$. A larger value for l_n^* results in smaller lever length with the consequence for the yielding to require a larger external force, which again leads to an increase of the plateau value as shown in Fig. 4a.

It can be noticed from Fig. 4a, that the stiffness ratio lies consistently above the strength ratio for the given low r/l ratio of 0.19. For the results of larger r/l ratios of 0.25 and 0.31, it was found that the stiffness ratio is consistently below the strength ratio. This discrepancy cannot be resolved by adjusting the geometrical parameters r_n^* and l_n^*. For avoiding a more refined geometrical modeling of the nodal area which might lead to too many parameters and dependencies, it is feasible to additionally use the Young's modulus assigned to the beam elements in the nodal area, E_n^*, to independently adjust the effective stiffness of the nodal area. Therefore, with the three adjustable parameters r_n^*, l_n^* and E_n^*, a general fitting approach can be conducted according to the following steps:

a) The magnitude of l_n^* is determined such that the strength plateau (red circles in Fig. 4a) lies on or slightly above the desired reference value $F_{beam}/F_{solid} \geq 1$ represented by the yellow plane in Fig. 4a. This is done by tuning the number of beam elements included in the nodal area, assigned with the nodal radius, r_n^*, while the remaining elements keep the radius of the ligament, r.
b) r_n^* is secondly adjusted for the beam model to reproduce the correct strength of the solid model such that $F_{beam}/F_{solid} = 1$.
c) The final calibration of E_n^* will resolve the remaining calibration of the stiffness $k_{beam}/k_{solid} = 1$ without affecting the strength that was calibrated before.

According to the steps listed above, for the case shown in Fig. 4a, firstly $l_n^*/l_n = 2.23$ is determined, which is followed by the determination of $r_n^*/r = 1.4$. The fitting is completed by adjusting E_n^* to $E_n^*/E_s = 0.75$ and, as illustrated in Fig. 4b, a 99% agreement is simultaneously reached for the stiffness and strength ratio, marked by the rectangle in Fig. 4b. It should noted that an exact match in step a) is nor required neither desired, because we want to use the initial discretization of the ligament to form the elements in the nodal areas in the randomized RVEs structures. Other approaches with variable element length are also possible, but would need a remeshing of nodal area as well as the remaining ligament.

All nine geometries listed in Table 1 were analyzed following the steps introduced above. An overall fitting accuracy of 98% is achieved simultaneously for stiffness and strength. The results shown in Fig. 5a–d are presented in form of the ratios of the adjustable parameters of the nodal corrected beam model to the corresponding parameters of the solid model, l_n^*/l_n, l_n^*/l, r_n^*/r, and E_n^*/E_s respectively. These ratios can be interpreted as indicators for the geometrical difference of the nodal

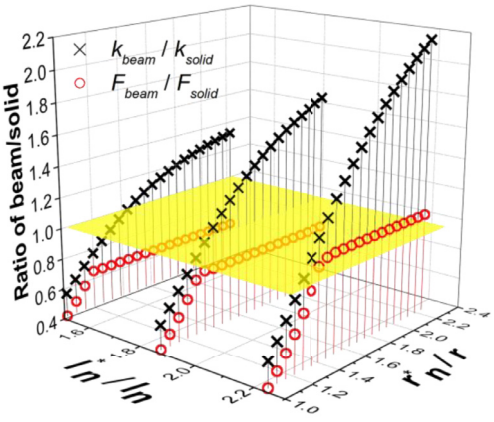

(a)

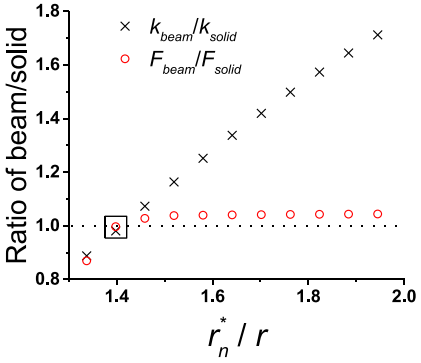

(b)

Fig. 4. Comparison of the mechanical response obtained for the beam and solid model for the case $r/l = 0.19$ and $c_R = 1.1$. (a) Scan with variation of geometrical parameters r_n^* and l_n^*; best agreement is achieved along the curve $l_n^*/l_n = 2.23$ at $r_n^*/r = 1.4$; (b) Final fitting with 99% accuracy of stiffness and strength by additionally adjusting the material parameter E_n^* to $E_n^*/E = 0.75$.

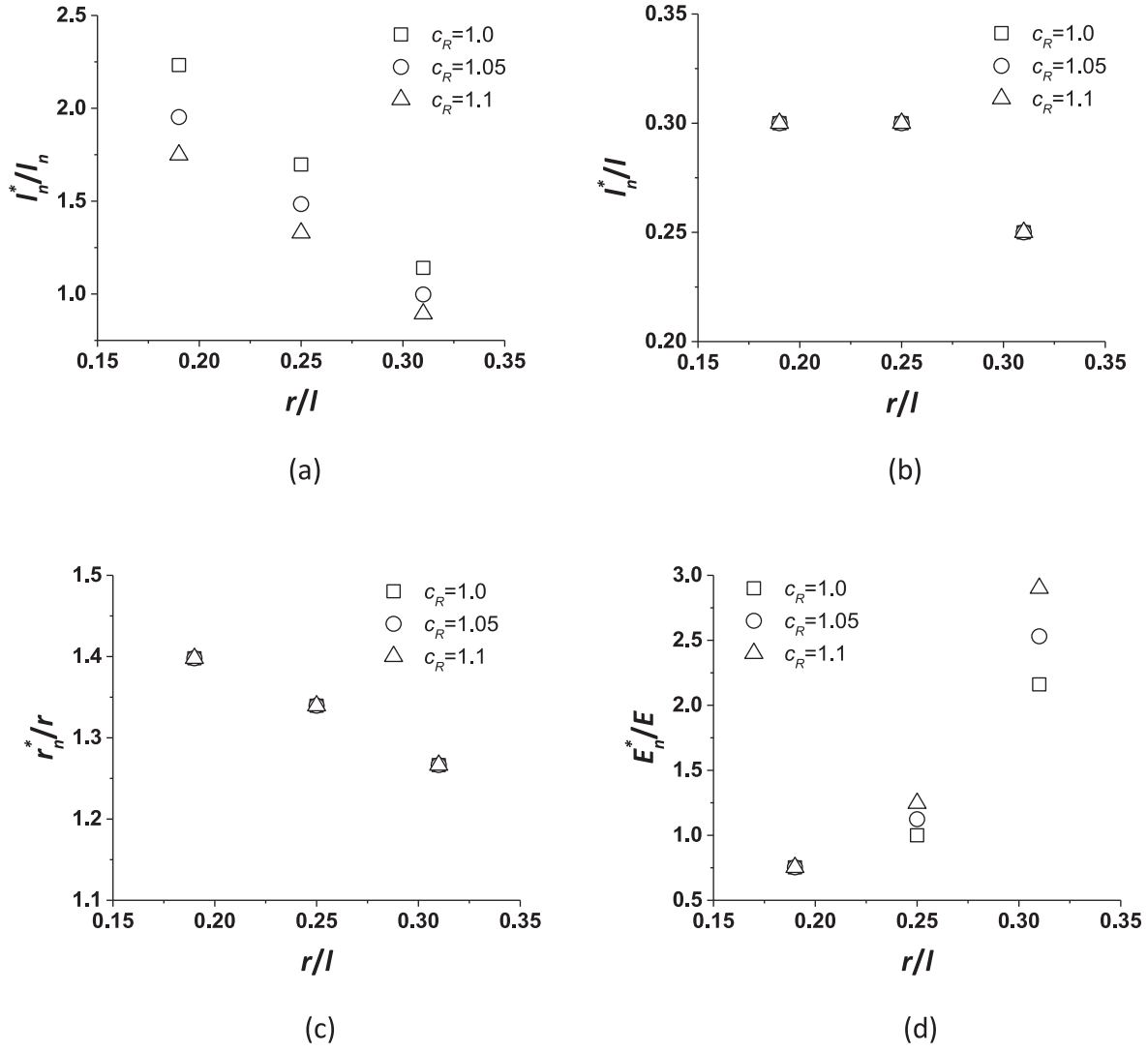

Fig. 5. Identified values for the adjustable parameters of the nodal beam elements providing an 98% agreement of the tetrahedron beam model with the solid model with respect to stiffness and strength for the cases listed Table 1 (a) l_n^*/l_n; (b) l_n^*/l; (c) r_n^*/r; and (d) E_n^*/E_s ratio.

area modeled by beam elements such that it predicts the macroscopic response of a solid model. Fig. 5a shows that the value of l_n^*/l_n is strongly dependent on the r/l ratio and c_R. As it is further shown in Fig. 5b, the magnitude of l_n^*/l (l is kept constant) for a given r/l does not depend on c_R. This shows that the dependency of l_n^*/l_n on c_R shown in Fig. 5a is caused by the calculation of the l_n values as function of c_R. The decrease of l_n^*/l_n from 2 ± 0.2 to 1 ± 0.1 in Fig. 5a suggests that the size of the nodal area is converging with increasing ligament size. In other words, the beam model's plastic behavior based on the same geometry is closer to that of the solid model for larger ligament sizes (this is further discussed in sect. 4.1). The same line of arguments applies to the ratio r_n^*/r, see Fig. 5c.

The third adjustable material parameter, E_n^*, controls the elastic behavior of the nodal area. Fig. 5d demonstrates a general trend that the ratio of E_n^*/E_s increases from 0.75 for $r/l = 0.19$ to 2.5 ± 0.04 for $r/l = 0.31$. The required correction of the effective nodal stiffness increases progressively with increasing r/l ratio and, at the same time, it shows an increasing sensitivity with regard to the nodal extension, represented by c_R. The general trend from a value below 1 to increasing values simply results from the discrepancy between the stiffness and strength ratio that has been discussed in context of Fig. 4a. That ratio follows the opposite and has to be compensated by an increasing local Young's modulus assigned to the nodal beam elements.

Eqs (1)–(3) are the fitting functions that are generated based on the date sets from Fig. 5(a), (c) and (d), respectively. The fitting constants are listed in Table 2.

$$l_n^*/l_n = a_0 + a_1 \cdot r/l \tag{1}$$

$$r_n^*/r_n = a_0 + a_1 \cdot r/l \tag{2}$$

$$E_n^*/E = a_0 + a_1 \cdot \exp(a_2 \cdot r/l) \tag{3}$$

2.3. Model validation

It was reported in the work of [18] that besides bending as the major deformation mechanism, torsion represents another fundamental deformation that is caused by the spatially curved ligaments and should not be neglected. The torque in the ligaments occupies approx. 20% of ligament loading under macroscopic compressing of nanoporous gold. The validation of the proposed model is therefore firstly comparing the nodal corrected beam tetrahedron model to the solid model, see Fig. 1, under external torsion loading.

Fig. 6 shows the comparison between solid model (SM) and beam tetrahedron under torsion. The torque M_t has been normalized with Er^3.

Table 2
Fitting constants for Eqs (1)–(3).

	l_n^*/l_n (Eq. (1))			r_n^*/r_n (Eq. (2))	E_n^*/E (Eq. (3))		
	$c_R = 1.0$	$c_R = 1.05$	$c_R = 1.1$	$c_R = 1.0,1.05,1.1$	$c_R = 1.0$	$c_R = 1.05$	$c_R = 1.1$
a_0	3.97	3.47	3.11	1.61	0.69	0.62	0.54
a_1	-9.10	-7.96	-7.13	-1.09	4.97E-4	1.93E-3	4.57E-3
a_2					25.79	22.25	20.15

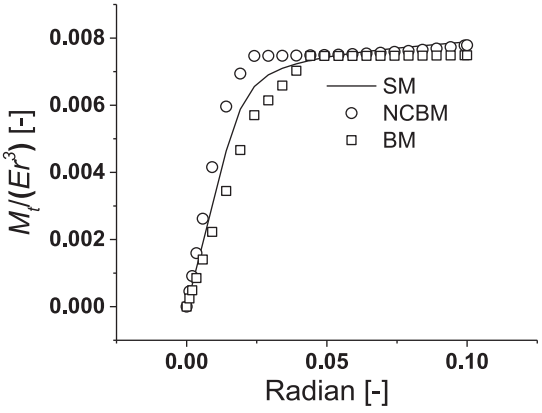

Fig. 6. The mechanical responses of solid model (SM), beam model (BM) and nodal corrected beam model (NCBM) for the tetrahedron structure under external torsion loading for the case of $r/l = 0.25$, $c_R = 1.1$.

The overall fitting of the nodal corrected beam model (NCBM) is comparable to that of the beam model (BM), reaching a beam to solid stiffness ratio of 130% and an approx. 80% overall accuracy for the plastic deformation. The performance for torsion was found to be consistent across the whole range of r/l studied in the current work. As in randomized RVEs approx. 80% of the ligament deformation is originating from bending as the governing deformation mechanism and approx. 20% is related to torsion [18], it is reasonable to assume that the overall error in the macroscopic response of the RVE is kept within 10%.

As discussed in the introduction, the RVE beam model provides an ideal access for studying the mechanics of nanoporous materials. In contrast to the analyzes based on a building block, an RVE however contains thousands of ligaments interconnected in a network structure. Such a network structure is much more representative of the real material in terms of structural features, local loading of the ligaments as well as observable deformation mechanisms. The current nodal correction method is therefore integrated into the RVE beam model using the diamond structure, developed in the work of [8]. Three RVEs have been generated as solid and beam models for $c_R = 1.1$ and ligament aspect ratios of $r/l = 0.19$, 0.25, and 0.31. In Fig. 7a and b the RVEs are shown for $r/l = 0.25$ for the solid and the beam model (in rendering mode), respectively. The RVEs are loaded with the same compression deformation of 25% engineering strain on the top surface. Although the structure is perfectly ordered, it represents a further step of validation, because the macroscopic compression of the RVE translates into a different local load distribution and deformation in the tetrahedrons as applied during the calibration of the nodal corrected elements.

The resulting agreement for the macroscopic elastic modulus between the beam and solid RVE is $100 \pm 5\%$ for all three cases. Thus, the nodal corrected beam model is capable of predicting the elastic mechanical response of the RVE equivalently to the solid model.

Because an elastic-perfectly plastic material model is used so far, early convergence problems have been faced in all beam RVE simulations, possibly owing to buckling. Therefore, a more realistic elastic-linear plastic constitutive law is employed to the simulations of RVEs for both of the beam and solid models, using the same elastic properties $E_s = 81$ GPa, $\nu = 0.42$, along with yield stress $\sigma_{y,S} = 500$ MPa, but a non-zero work hardening rate γ of 1000 MPa [8,13]. Besides the consideration for resolving convergence problems, the application of the elastic-linear plastic material model is also motivated by the purpose of examining the generality of the nodal corrected beam modeling concept in presence of work hardening.

Fig. 8a demonstrates the resulting macroscopic stress-strain response from the nodal corrected beam RVE and the solid model RVE for different r/l ratios in comparison with the results from the original beam model. The nodal corrected beam model (NCBM) significantly improves the predictions of the macroscopic mechanical response by eliminating the systematic underestimation of stiffness and strength of the original beam model (BM). Furthermore, a very good agreement with the solid model (SM) is achieved over the whole strain range. Fig. 8b shows the ratio of the resulting reaction force obtained for the nodal corrected beam RVE and the solid model RVE against the macroscopic compression strain, ε_{eng}. The overall error of the elastic-plastic response of the nodal corrected beam RVE is within about 10% for all solid fractions (i.e. all considered r/l ratios). More specifically, the accuracy is $101\% \pm 5\%$ for $r/l = 0.19$ and 0.31, and $103\% \pm 7\%$ for $r/l = 0.25$. It can be concluded that the nodal corrected beam model provides a sufficiently accurate elastic-plastic mechanical response that has the same predictive quality of a corresponding solid model. At the same time it costs much less computation time and provides much more degrees of freedom concerning the introduction of a random structure [8,29] as well as variation of ligament shapes in the RVE [18].

3. Discussion of scaling laws

In this section we will apply the nodal corrected beam RVE proposed and validated in the previous sections for analyzing the impact of the nodal correction on the scaling laws for Young's modulus and strength. The resulting curves are compared to scaling laws from literature. For the nodal corrected beam RVE, the solid fraction φ is derived from the original geometry that corresponds to the solid RVE.

Fig. 9a and b represent the scaling behavior of the macroscopic Young's modulus and strength that are computed from the RVE normalized to the corresponding material properties of the solid fraction in the form E/E_S, and $\sigma_y/\sigma_{y,S}$, respectively. The curves are shown in comparison with scaling laws suggested in previous works [8,29], as well as the original Gibson-Ashby scaling laws that serve as the common reference for all models. For open pore foams that imply bending as major deformation mechanism, the leading constants in Eqs. (4) and (5) are $C_E = 1$ and $C_\sigma = 0.3$ respectively [10].

$$E/E_S = C_E \varphi^2 \tag{4}$$

$$\sigma_y/\sigma_{y,S} = C_\sigma \varphi^{3/2} \tag{5}$$

In Fig. 9a, the scaling behavior of the Young's modulus, E/E_S, calculated from the different RVEs is plotted against the solid fraction φ. The different φ values are the results of varying r/l ratios with 0.19, 0.25 and 0.31, given in Table 1. The black solid line corresponds to Eq. (11) in [8] which describes the scaling law of the RVE beam model under consideration of the effect of shear deformation for thick beams, i.e. it is the approximation of the lower bound for the diamond RVE. The diamond

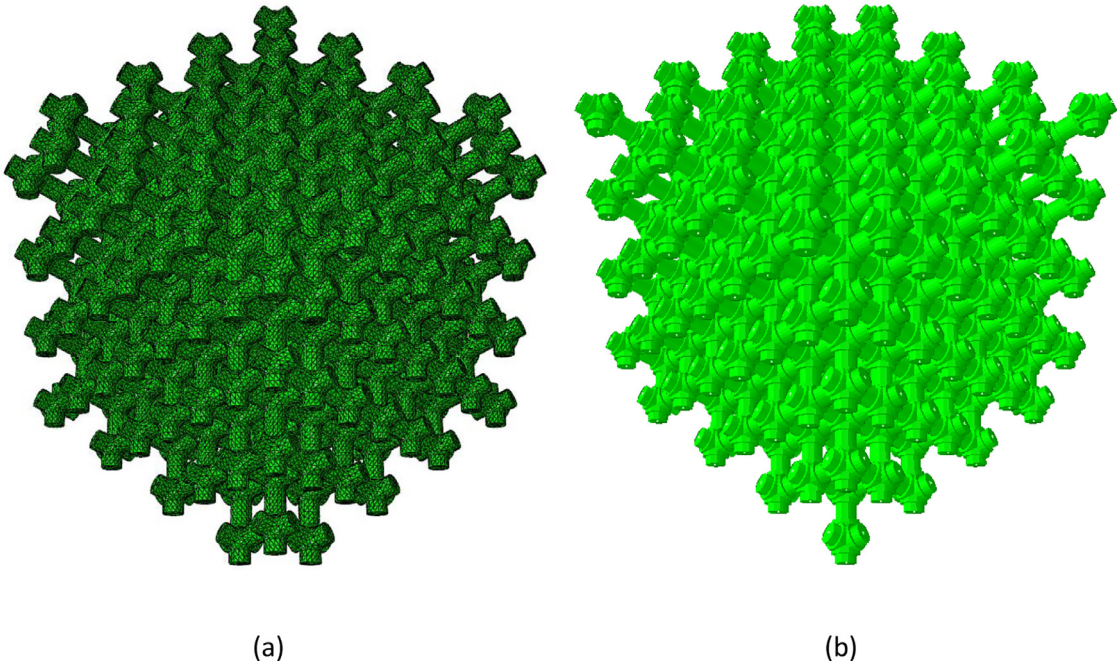

Fig. 7. RVEs for $r/l = 0.25$ and $c_R = 1.1$ (a) solid model; (b) nodal corrected beam model with the same effective elastoplastic response.

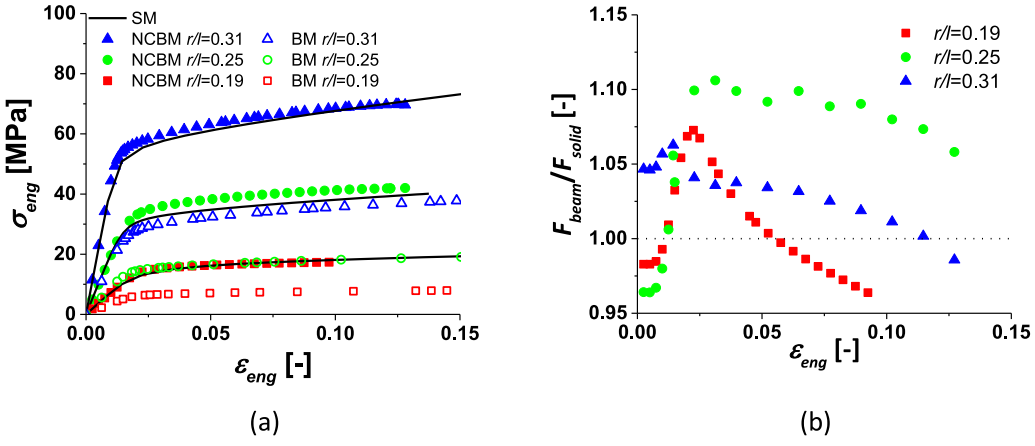

Fig. 8. (a) Macroscopic stress-strain response for RVEs built as solid model, beam model, and nodal corrected beam model for various r/l ratios; (b) RVE reaction force ratios F_{beam}/F_{solid} for different r/l values covering the whole range of elastic and elastic-plastic deformation.

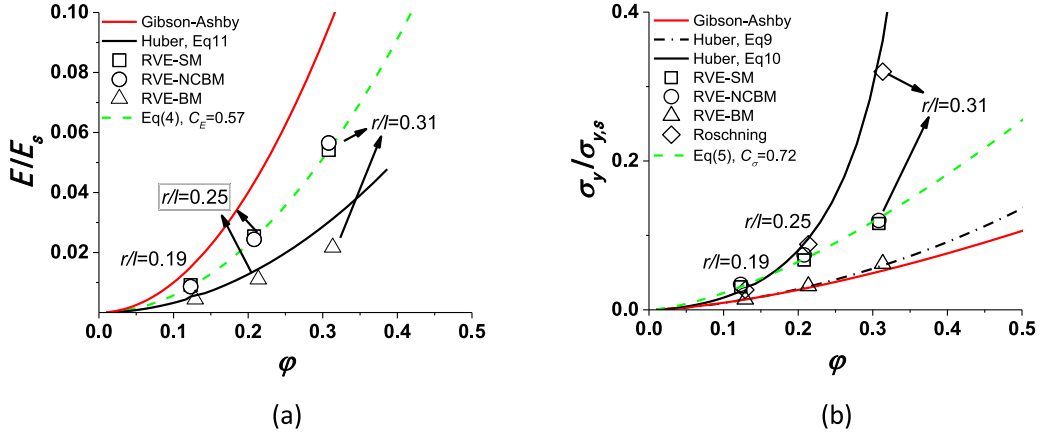

Fig. 9. Comparison between the nodal corrected beam model and previous studies for (a) Young's modulus; (b) yield strength. RVE-SM, RVE-NCBM, and RVE-BM denote the results from the RVE solid model (this work, Fig. 7a), the RVE nodal corrected beam model (this work, Fig. 7b) and RVE beam model [29], respectively. All results are for perfectly ordered diamond structure ($A = 0$).

unit cell is more compliant than that by Gibson and Ashby, which explains the comparably low stiffness also for smaller solid fractions. The RVE nodal beam model (RVE-BM) reproduces the agreement between the scaling law and the numerical results as in [8].

The results from the nodal corrected beam model developed in this work, represented by the circles (RVE-NCBM), show an increase by approx. a factor of two compared to the beam model (RVE-BM). The data from the solid model (squares, RVE-SM) confirm the level of accuracy that is achieved by the incorporation of the nodal correction in the RVE.

The results of the nodal corrected beam model lead to a scaling relation that can be fitted by **Eq. (4)** with $C_E = 0.57$, entered as green dashed line in **Fig. 9**a. It is understood that this is still describing a perfect diamond unit cell. However, the structure of nanoporous metals is distorted and ligaments are curved and varying in aspect ratio. Previous studies showed that randomization of the structure leads to a further increase in compliance [8,29]. In recent studies [14,30], experimentally constructed scaling relations are developed for the macroscopic Young's modulus of nanoporous gold, which suggest the power in **Eq. (4)** being 2.5 or 2.8 with $C_E = 1$ or 0.86. However, the incorporation of the nodal mass in this work does not lead to an exponent different to 2 that according to [10] represents the highest power of all types of deformation (tension, compression, shear, bending). At this point the question remains unsolved how higher values in the exponent, as observed from experiments, can be explained by a structural model such as the RVE presented in this work.

Fig. 9b shows the results for the scaling behavior of the yield strength σ_y, normalized by the yield strength of the solid phase $\sigma_{y,S}$. Again, the analytical solution for the beam model proposed as Eq. (9) in [8] provides a lower limit that corresponds to the numerical results from the beam model (RVE-BM). It can be also observed that the Gibson-Ashby model with $C_\sigma = 0.3$ results in a good agreement with that scaling relation.

The analytical nodal correction (black solid line) proposed in the work of [8] as Eq. (10) forms the upper limit which agrees well with the results from the work of [29] represented by rhombus symbols in **Fig. 9**b. In [8] the macroscopic strength for the RVE beam model was corrected by reducing the available lever for bending of the ligament by the radius of the nodal mass. In [29] this effect was translated into the beam model by increasing the yield strength of the solid fraction according to this structural strengthening effect. The latter approach has the advantage, that it does not affect the stiffness of the network structure. For both of the works, the nodal mass is taken account as a shortening of the effective bending lever of the ligaments and assuming that yield occurs at the edge formed by the ligament and the node. The results shown in **Fig. 9**b lead to the conclusion that this type of correction provides reasonable results for solid fractions $\varphi \leq 0.15$. It however significantly overestimates the effect of the nodal mass on the macroscopic strength for $\varphi > 0.15$, which is where the nanoporous metals are located. In view of these insights, we will revisit the analysis of [8] and [29] with support of the nodal corrected beam model in Sect.4.2.

The results of the nodal corrected beam RVE-NCBM (black circles) initially follow the solution for the upper limit but then deviate by continuing in a much less progressive way for $\varphi > 0.15$. This is because that the upper limit is constructed under the assumption that the plastic deformation will always happen at the end of the ligament that is analytically shortened for the presence of a node. This means that the nodal area for this upper limit is set to be infinitely strong, e.g. no plastic deformation can happen within the nodal area. However, the visual investigation on the local plastic deformation of the nodal corrected beam model and solid model indicates that, the nodal area is also plastically deformed. This trend becomes more significant with increasing φ, because larger solid fractions lead to less geometrical distinction r_n^*/r between the nodal area and the ligament as shown in **Fig. 5**c. So that the nodal corrected model tends to predict a much lower strength at a higher φ. A fit of the data using the scaling law, **Eq. (5)** (green dashed line) leads to a leading constant $C_\sigma = 0.72$. The increase of the leading constant C_σ from 0.3 (Gibson-Ashby) to 0.72 (RVE-NCBM) demonstrates that the nodal mass strengthens the diamond structure by a factor of more than two.

4. Application in randomized RVEs

4.1. Effect of nodal mass for randomized structures

Up to this point, the diamond RVE was used with the purpose of a clean assessment of the effect of the nodal mass on the scaling relations. For investigating the new possibilities of the nodal corrected beam elements for a more realistic nanoporous structure, the randomization parameter A [8] is included in the RVE. This parameter defines a random displacement applied to each connecting node, leading to a spatial curvature of the connected ligaments. The parameter A defines the fraction of the amplitude of the equally distributed random displacement in relation to the unit cell size of the undistorted diamond unit cell. The effect of the randomization level on the solid fraction φ, caused by the spatial lengthening of the ligaments, has been taken into account in the following analyzis as suggested by [8,29]. Concerning the macroscopic response of the RVE, increasing randomization decreases the values of E and σ_y, as well as the degree of lateral extension. For more details we refer to [8,29].

For the nodal corrected beam model, the randomization characteristics are also introduced to the nodal areas because the lengthening of the elements applies to all elements of the model. This gives rise to the question if the lengthening of the elements caused by the randomization should be kept as is or if it should be avoided in the nodal areas of the nodal corrected beam model. For what follows, we assume that the nodal element properties follow the relationships that shown in **Fig. 5**. This means that for a given ratio of l_n^*/l_n an increase in the ligament length l_n, caused by the randomization, leads to a proportional increase in the nodal element length l_n^*. It is thus consistent to let the nodal elements elongate in the same way as the elements that form the ligament. As the purpose of the introduction of nodal corrected beam elements exclusively aims at a mechanically equivalent behavior with reference to the solid model, the calculation of the solid fraction remains unaffected.

All simulations for randomized structures are carried out for $c_R = 1.1$. Each data point plotted in **Fig. 10** represents the average of five realizations; the size of the error bar corresponds to the standard deviation. **Fig. 10**a shows the ratio of the macroscopic Young's modulus of the nodal corrected beam model, E_{NCBM}, to beam model, E_{BM}, with respect to various randomization levels from $A = 0$ that is perfect ordered to $A = 0.3$ that is strongly disordered. It is shown that for all randomization levels the stiffness ratio increases nearly linearly with the solid fraction, indicating the contribution of the nodal mass to the stiffness. Moreover, with increasing randomization level the curves shift right and down. The right shift is due to the increase of solid fraction that is caused by the increase of the randomization level. The trend of slightly shifting downwards reveals the effect of the degree of randomization on the compliance in the nodal areas, which is slightly reducing the nodal mass contribution on the macroscopic elasticity. This effect is about 10% if we consider the full range from zero to maximum randomization.

The vertical axis of **Fig. 10**b demonstrates the ratio of the yield strength of the nodal corrected beam model $\sigma_{y,NCBM}$ to the beam model $\sigma_{y,BM}$ with respect to various randomization levels. The general trend of **Fig. 10**b to a is opposite, namely, increasing solid fraction leads to a relative decrease of the contribution of nodal mass to the macroscopic strength. For better understanding of this effect, the linkage between the current discussion to the discussions of **Fig. 5**a, b and c is required. In the discussion of **Fig. 5** it was stated that with increasing r/l the geometrical gap between a cylindrical shaped node and an actual spherical node response is closing with increasing solid fraction, i.e. $l_n^*/l_n \to 1$ and $r_n^*/r_n \to 1$. It can be also be observed that the strength ratio gradually shifts downwards from 2.5 to 2 for $A = 0$ and from 1.8 to 1.5 for $A = 0.3$. Because the plastic deformation initiates in the transition from the nodal

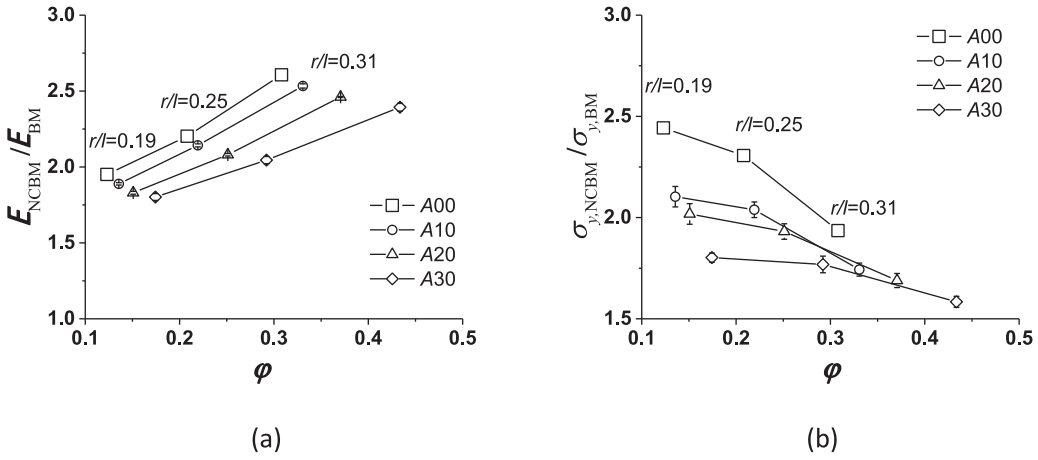

Fig. 10. Results for the macroscopic properties of the randomized RVE as ratio of the nodal corrected beam model (NCBM) to the beam model (BM) (a) Young's modulus; (b) yield strength.

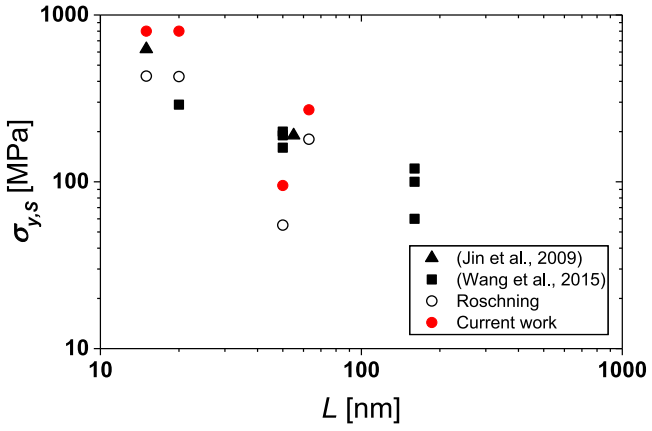

Fig. 11. Determined yield strength of the solid phase vs. ligament size, L. Experimental data are taken from [32,33]; model data from [29].

area to the ligament, the effect on the strength reduces with reducing size of the nodal elements. With increasing degree of randomization, the correlation between local geometry and macroscopic strength is more and more reduced and becomes weak for $A = 0.3$ and solid fractions of $\varphi \leq 0.3$.

4.2. Analysis of experimental data

To evaluate the performance of the nodal corrected beam model the size dependent yield strength of the ligaments is determined from literature data on macroscopic compression of nanoporous gold samples with different ligament size.

In the work of [29], the scaling relation for the macroscopic yield strength was used as the starting point for fitting the true stress-strain curves obtained from macroscopic compressing nanoporous gold samples with various ligament size [31,32] using the RVE model. The outcomes that were from the fitting were a data set of yield strengths for the solid phase $\sigma_{y,S}$ in dependence of ligament size, represented by hollow circles in **Fig. 11**. This data set is plotted against results from the works of [32,33] as solid black symbols in **Fig. 11**, that were determined using independent approaches. Roschning et al.'s results are of the same magnitude as those data reported in the referenced literatures, but one result for the 50 nm ligament size appeared to be an outlier which could not be explained by [29]. The only difference compared to the other data was that it had the highest solid fraction of all samples of $\varphi = 0.3$.

We re-analyzed the data with the nodal corrected RVE following the same approach proposed by [29] with a randomization level of $A = 0.23$ and a ligament aspect ratio of $r/l = 0.25$. The results, shown as solid red symbols in **Fig. 11**, lead to an elevation of Roschning et al.'s results. The nodal corrected beam RVE seems to provide an overall closer alignment with the results from [32,33]. In particular, the previous outlier is now closer to the overall trend.

The different elevation in the yield strength for the different data points can be understood with the help of **Fig. 9**b. The nodal correction applied in [29] was based on a correction term which – as a result of the assumed rigidity of the nodal mass – increasingly overestimates the geometrical strengthening for increasing solid fraction. Because the materials yield strength and the geometrical strengthening effect are multiplicative with respect to the macroscopic strength, a reduction of the geometrical strengthening effect to the accurate value must be compensated by an increased yield strength of the solid fraction, $\sigma_{y,S}$. The higher the solid fraction, the more the identified yield strength is elevated. Consequently, the original outlier, which has the highest solid fraction, gets mostly elevated.

5. Conclusions

In the current work, a new beam modeling concept for nanoporous metals has been proposed for predicting the macroscopic elastic-plastic response by incorporating the connecting nodal mass in the junctions of the network structure. The nodal corrected beam model is calibrated based on the mechanical response for bending of a beam tetrahedron structure in relation to its corresponding solid model by adjusting three additional parameters specifically assigned to the nodal area. An excellent agreement between the nodal corrected beam and solid RVE for elastic modulus and yield strength has been achieved, which is conducted without losing the advantage of the high computational efficiency.

The nodal correction leads to an increase in the macroscopic stiffness and strength of the beam model. The leading constant in the resulting scaling law for Young's modulus is $C_E = 0.57$ and, compared to the beam model without nodal correction, about a factor of two larger. It is however still less stiff than the original Gibson-Ashby model that has a leading constant of $C_E = 1$. The incorporation of the nodal mass does not change the exponent of 2 in the scaling law.

With respect to macroscopic plastic deformation, the correction suggested in [8,29] significantly overestimates the effect of the nodal mass for solid fractions above 15%. It was found, that the scaling law of Gibson-Ashby very well fits the data from the simulations with the nodal corrected RVE, when the leading constant is set to be $C_\sigma = 0.72$. This difference to [8] is now understood as a consequence of the overestimation

of the effect of the nodal mass on the structural strength by the proposed correction term for solid fractions above 15%. After re-analyzing the literature data with the nodal corrected beam model RVE, the overall agreement of the size dependent yield strength from different sources is improved.

In line with the referenced literatures, the present work demonstrates once more the importance of local geometric features in terms of the macroscopic mechanical response of nanoporous metals. The nodal correction proposed in this work is one important element in addition to randomization and local ligament size variation. A further development of this modeling approach will offer various possibilities for the implementation of further details without losing its efficiency.

Acknowledgments

Support was provided by Deutsche Forschungsgemeinschaft within SFB 986 "Tailor-Made Multi-Scale Materials Systems: M^3", project B4.

Appendix A. Nomenclatures

Parameters	Descriptions
φ	Solid fraction
w	Transverse loading displacement
R	Nodal radius
l_n	Length between nodal center and the end of the ligament attached to the node
r_n^*	Larger cross-section radius of beam element in the nodal area (adjustable)
l_n^*	The length between the node center and the end of the ligament (adjustable)
r	Ligament radius
l	Ligament length
c_R	Constant governing nodal mass
R	Nodal radius
E_S	Young's modulus
ν	Poisson's ratio
$\sigma_{y,S}$	Yield strength
k_{solid}	Stiffness of the solid tetrahedron
F_{solid}	Solid tetrahedron strength
k_{beam}	Stiffness of the beam tetrahedron
F_{beam}	Beam tetrahedron strength
E_n^*	Young's modulus for the beam elements of nodal area (adjustable)
a_0, a_1, and a_2	Constants for fitting functions Eqs (1)–(3)
ε_{eng}	RVE macroscopic compression engineering strain
C_E and C_σ	Constants of Gibson-Ashby model
A	Randomization parameter
E_{NCBM}	Macroscopic Young's modulus of nodal corrected beam model
E_{BM}	Macroscopic Young's modulus of beam model
$\sigma_{y,NCBM}$	Macroscopic yield strength of nodal corrected beam model
$\sigma_{y,BM}$	Macroscopic yield strength of beam model

References

[1] Weissmüller J, Newman RC, Jin H-J, Hodge AM, Kysar JW. Nanoporous Metals by Alloy Corrosion: Formation and Mechanical Properties. MRS Bulletin 2009;34(08):577–86.
[2] Balk TJ, Eberl C, Sun Y, Hemker K, Gianola D. Tensile and compressive microspecimen testing of bulk nanoporous gold. JOM 2009;61(12):26–31.
[3] Biener J, Hodge AM, Hayes JR, Volkert CA, Zepeda-Ruiz LA, Hamza AV, et al. Size effects on the mechanical behavior of nanoporous Au. Nano Lett 2006;6(10):2379–82.
[4] Biener J, Hamza A, Hodge A. Deformation behavior of nanoporous metals. Micro and nano mechanical testing of materials and devices. Springer; 2008. p. 118–35.
[5] Roberts A, Garboczi EJ. Elastic properties of model random three-dimensional open–cell solids. J Mech Phys Solids 2002;50(1):33–55.
[6] Sun X-Y, Xu G-K, Li X, Feng X-Q, Gao H. Mechanical properties and scaling laws of nanoporous gold. J Appl Phys 2013;113(2):023505.
[7] Mangipudi KR, Epler E, Volkert CA. Morphological similarity and structure-dependent scaling laws of nanoporous gold from different synthesis methods. Acta Materialia 2017;140:337–43 (Supplement C).
[8] Huber N, Viswanath RN, Mameka N, Markmann J, Weißmüller J. Scaling laws of nanoporous metals under uniaxial compression. Acta Materialia 2014;67:252–65.
[9] Pia G, Delogu F. Nanoporous Au: Statistical analysis of morphological features and evaluation of their influence on the elastic deformation behavior by phenomenological modeling. Acta Materialia 2015;85:250–60.
[10] Gibson LJ, Ashby MF. Cellular solids: structure and properties. Cambridge university press; 1997.
[11] Balk TJ, Eberl C, Sun Y, Hemker KJ, Gianola DS. Tensile and compressive microspecimen testing of bulk nanoporous gold. JOM 2009;61(12):26–31.
[12] Liu R, Antoniou A. A relationship between the geometrical structure of a nanoporous metal foam and its modulus. Acta Materialia 2013;61(7):2390–402.
[13] Hu K, Ziehmer M, Wang K, Lilleodden ET. Nanoporous gold: 3D structural analyses of representative volumes and their implications on scaling relations of mechanical behaviour. Philosophical Magazine 2016:1–14.
[14] Badwe N, Chen X, Sieradzki K. Mechanical properties of nanoporous gold in tension. Acta Materialia 2017;129:251–8.
[15] Farkas D, Caro A, Bringa E, Crowson D. Mechanical response of nanoporous gold. Acta Materialia 2013;61(9):3249–56.
[16] Ngô B-ND, Stukowski A, Mameka N, Markmann J, Albe K, Weissmüller J. Anomalous compliance and early yielding of nanoporous gold. Acta Materialia 2015;93:144–55.
[17] Ngô BND, Roschning B, Albe K, Weissmüller J, Markmann J. On the origin of the anomalous compliance of dealloying-derived nanoporous gold. Scripta Materialia 2017;130:74–7.
[18] Jiao J, Huber N. Deformation mechanisms in nanoporous metals: Effect of ligament shape and disorder. Comput Mater Sci 2017;127:194–203.
[19] Lührs L, Soyarslan C, Markmann J, Bargmann S, Weissmüller J. Elastic and plastic Poisson's ratios of nanoporous gold. Scripta Materialia 2016;110:65–9.
[20] Saane SSR, Mangipudi KR, Loos KU, De Hosson JTM, Onck PR. Multiscale modeling of charge-induced deformation of nanoporous gold structures. J Mech Phys Solids 2014;66:1–15.
[21] Soyarslan C, Husser E, Bargmann S. Effect of Surface Elasticity on the Elastic Response of Nanoporous Gold. Journal of Nanomech Micromech 2017;7(4):04017013.
[22] Husser E, Soyarslan C, Bargmann S. Size affected dislocation activity in crystals: Advanced surface and grain boundary conditions. Extreme Mech Lett 2017;13:36–41.
[23] Bargmann S, Soyarslan C, Husser E, Konchakova N. Materials based design of structures: Computational modeling of the mechanical behavior of gold-polymer nanocomposites. Mech Mater 2016;94:53–65.
[24] Lührs L, Müller B, Huber N, Weissmüller J. Plastic Poisson's Ratio of Nanoporous Metals: A Macroscopic Signature of Tension-Compression Asymmetry at the Nanoscale. Nano Lett 2017;17:6258–66.
[25] Pia G, Delogu F. Mechanical behavior of nanoporous Au with fine ligaments. Chem Phys Lett 2015;635:35–9.
[26] Ziehmer M, Hu K, Wang K, Lilleodden ET. A principle curvatures analysis of the isothermal evolution of nanoporous gold: Quantifying the characteristic length-scales. Acta Materialia 2016;120:24–31.
[27] Mangipudi KR, Epler E, Volkert CA. Topology-dependent scaling laws for the stiffness and strength of nanoporous gold. Acta Materialia 2016;119:115–22.
[28] DassaultSystèmes. Abaqus Documentation 2014.
[29] Roschning B, Huber N. Scaling laws of nanoporous gold under uniaxial compression: Effects of structural disorder on the solid fraction, elastic Poisson's ratio, Young's modulus and yield strength. J Mech Phys Solids 2016(92):55–71.
[30] Zabihzadeh S, Van Petegem S, Holler M, Diaz A, Duarte LI, Van Swygenhoven H. Deformation behavior of nanoporous polycrystalline silver. Part I: Microstructure and mechanical properties. Acta Materialia 2017;131:467–74.
[31] Wang K, Weissmüller J. Composites of Nanoporous Gold and Polymer. Adv Mater 2013;25(9):1280–4.
[32] Wang K, Kobler A, Kübel C, Jelitto H, Schneider G, Weissmüller J. Nanoporous–gold-based composites: toward tensile ductility. NPG Asia Mater 2015;7(6):e187.
[33] Jin H-J, Kurmanaeva L, Schmauch J, Rösner H, Ivanisenko Y, Weissmüller J. Deforming nanoporous metal: Role of lattice coherency. Acta Materialia 2009;57(9):2665–72.